

Determination of Ω_b From Big Bang Nucleosynthesis in the Presence of Regions of Antimatter

Elina Sihvola*

Department of Physics, University of Helsinki, P.O.Box 9, FIN-00014 University of Helsinki, Finland

Production of regions of antimatter in the early universe is predicted in many baryogenesis models. Small scale antimatter regions would annihilate during or soon after nucleosynthesis, affecting the abundances of the light elements. In this paper we study how the acceptable range in Ω_b changes in the presence of antimatter regions, as compared to the Standard Big Bang Nucleosynthesis (SBBN). It turns out that it is possible to produce at the same time both a low ${}^4\text{He}$ value ($Y_p < 0.240$) and a low D/H value ($\text{D/H} < 4 \times 10^{-5}$), but overproduction of ${}^7\text{Li}$ is unavoidable at large Ω_b .

PACS numbers: 26.35.+c, 98.80.Ft, 98.80.Cq, 25.43.+t

I. INTRODUCTION

Big Bang Nucleosynthesis (BBN) in the presence of regions of antimatter in a baryo-asymmetric universe has been studied recently in several papers, [1–4], first by Rehm and Jedamzik [1]. Production of antimatter domains is predicted in many baryogenesis models. If the universe is baryo-asymmetric and the domain structure is of the right distance scale, antimatter would get annihilated during or soon after nucleosynthesis, affecting the abundances of the light elements.

Annihilation after or shortly before recombination is strongly constrained by the Cosmic Microwave Background (CMB) and Cosmic Diffuse Gamma (CDG) radiation. If the antimatter regions are small enough to annihilate well before recombination, but after the weak freeze-out, the strongest constraint on the amount of antimatter is obtained from big bang nucleosynthesis. The relevant scales are $10^{-5} - 1$ pc.

In two earlier papers [2,3] we derived constraints on the antimatter fraction allowed by BBN observations. We fixed the mean baryon density to $\eta = 6 \times 10^{-10}$, corresponding to $\Omega_b h^2 = 0.022$. In this paper we extend the study to a range of values of η . We search for values of η that would be forbidden in the Standard Big Bang Nucleosynthesis (SBBN), but allowed in the presence of antimatter (antimatter nucleosynthesis, ABBN).

II. ANTIMATTER NUCLEOSYNTHESIS

A. Initial Conditions

We consider a situation where the early universe contains regions of antimatter, surrounded by a background of ordinary matter.

We model an antimatter region by a sphere with initially constant antibaryon density n_b . The antimatter sphere is surrounded by a spherical matter shell with equal baryon density. The initial structure is set by three parameters: 1) the antimatter fraction $R = f_v/(1 - f_v)$,

where f_v is the volume fraction of the antimatter region, 2) the net baryon density $\bar{n}_b = n_b(1 - R)/(1 + R)$, and 3) the physical radius of the antimatter region, r_A . The distances are given in comoving units in meters at $T = 1$ keV. One meter at $T = 1$ keV corresponds to 4.26×10^6 m today. The net baryon density \bar{n}_b is given as the baryon-to-photon ratio η today, which is related to Ω_b by $\eta = 274 \times 10^{-10} \Omega_b h^2$.

B. Lithium

We have studied BBN with antimatter regions in two previous papers [2,3]. We refer the reader to these papers for the details on physics and computations, and present in this paper only the new effects added since.

In our earlier papers we did not focus on lithium, whose observational limits are less secure than those of deuterium and helium. In this paper we consider also the production of ${}^6\text{Li}$ and ${}^7\text{Li}$.

The SBBN yield of ${}^6\text{Li}$ is small, ${}^6\text{Li}/\text{H} \sim 10^{-14}$. In the presence of antimatter additional ${}^6\text{Li}$ is produced by photodisintegration and annihilation of ${}^7\text{Li}$ and ${}^7\text{Be}$ and by non-thermal nuclear reactions.

About a half of the energy released in annihilation is carried away by photons and electrons, about a half by neutrinos, and a small fraction by nuclear debris. Energy release in the form of photons or electrons leads to ${}^6\text{Li}$ production via the nonthermal reactions ${}^4\text{He} + {}^3\text{H} \rightarrow {}^6\text{Li} + \text{n}$ and ${}^4\text{He} + {}^3\text{He} \rightarrow {}^6\text{Li} + \text{p}$, as first noted by Jedamzik [5]. The implications of this process on particle physics have been discussed by Jedamzik [5] and by Kawasaki *et al.* [6].

Photons and electrons initiate electromagnetic cascades, which first lose energy rapidly through photon-photon pair production and inverse Compton scattering. When the photon energies fall below $E_c = m_e^2/(80T)$, the photon-photon interactions cease and the thermalization continues much more slowly through pair production on a nucleus and Compton scattering on electrons. During this phase the photons may also photodisintegrate nuclei.

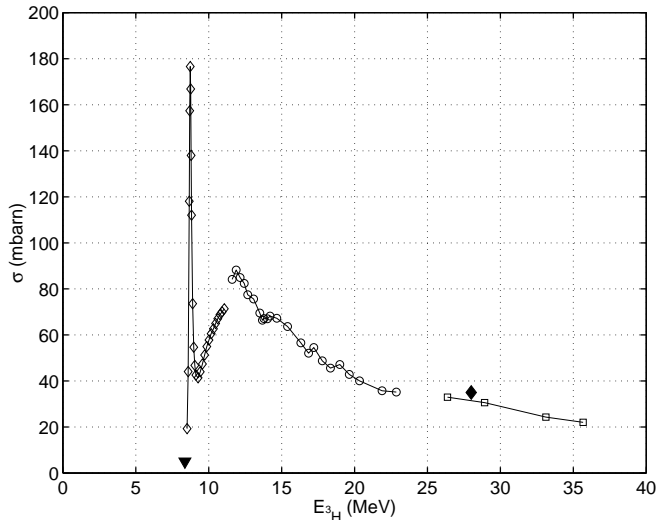


FIG. 1. Cross section of the ${}^4\text{He}({}^3\text{H}, \text{n}){}^6\text{Li}$ reaction, calculated from the cross section of the inverse reaction. The original ${}^6\text{Li}(\text{n}, \alpha){}^3\text{H}$ data: [8] (diamonds), [9] (circles), and [10] (squares). Not all the data points of the original papers have been included. The filled diamond presents the direct measurement by Koepke and Brown [7]. The threshold (8.39 MeV) is indicated by a triangle.

Photodisintegration of ${}^4\text{He}$ leaves energetic ${}^3\text{He}$ and ${}^3\text{H}$ ions, with energies up to $E_3 = (E_c - E_{\text{tr}})/4$, where $E_{\text{tr}} = 19.9(20.6)$ MeV is the threshold of the photodisintegration reaction ${}^4\text{He} + \gamma \rightarrow {}^3\text{H}({}^3\text{He}) + \text{p}(\text{n})$. These ions may further produce ${}^6\text{Li}$ via reaction ${}^4\text{He} + {}^3\text{H}({}^3\text{He}) \rightarrow {}^6\text{Li} + \text{n}(\text{p})$. The threshold of this reaction in the laboratory frame is 8.39 MeV for ${}^3\text{H}$ and 7.05 MeV for ${}^3\text{He}$. The photon energy must exceed 53.4(48.8) MeV in order to produce a ${}^3\text{H}({}^3\text{He})$ ion with energy above the threshold. The production of ${}^6\text{Li}$ begins when E_c rises above 48.8 MeV, i.e., when the temperature falls below $T = 67$ eV.

We get a smaller ${}^6\text{Li}$ production from ${}^4\text{He}$ photodisintegration than Jedamzik [5], by a factor of three. The difference is mainly due to Compton scattering, which was ignored in [5] in the thermalization of photons.

Also ${}^3\text{He}$ and ${}^3\text{H}$ ions from ${}^4\text{He} + \bar{p}(\bar{n})$ annihilation produce ${}^6\text{Li}$ via the same non-thermal reaction, as discussed by Rehm and Jedamzik [4]. The ${}^6\text{Li}$ ions produced by this process remain close to the annihilation zone, and are therefore more likely annihilated later, than the ${}^6\text{Li}$ ions from ${}^4\text{He}$ photodisintegration, which are distributed uniformly. Still, the annihilation-generated ${}^3\text{He}$ and ${}^3\text{H}$ dominate the production of ${}^6\text{Li}$.

We are aware of only one direct measurement on the cross section of the ${}^4\text{He} + {}^3\text{H} \rightarrow {}^6\text{Li} + \text{n}$ reaction [7]. Fortunately, there is data on the inverse reaction ${}^6\text{Li} + \text{n} \rightarrow {}^4\text{He} + {}^3\text{H}$. We use the principle of detailed balance to calculate the cross section of ${}^4\text{He} + {}^3\text{H} \rightarrow {}^6\text{Li} + \text{n}$ from its inverse reaction. The cross section is plotted in Fig. 1. For the ${}^4\text{He} + {}^3\text{He}$ reaction we use the same cross section,

shifted in energy according to the threshold energy.

The photodisintegration of ${}^6\text{Li}$ into the channel ${}^4\text{He} + \text{p} + \text{n}$ begins at $T = 0.88$ keV, and that of ${}^7\text{Li}({}^7\text{Be})$ at $T = 1.3(2.1)$ keV.

We have implemented into our code all the the ${}^6\text{Li}$ production processes described above. The slowing down of ions, the cascade spectrum, and the spectra of the annihilation debris are as in [3]. The photodisintegration reactions included in our code, together with references to the cross-section data, are given in Table I. We use the total single photoneutron cross-section ${}^7\text{Li}(\gamma, \text{n})\text{X}$ [11] for the ${}^7\text{Li}(\gamma, \text{n}){}^6\text{Li}$ reaction. In principle this leads to overestimation of the ${}^6\text{Li}$ production, since the reaction ${}^7\text{Li}(\gamma, \text{n})\text{X}$ may include other reaction channels. This is, however, unimportant, since the production of ${}^6\text{Li}$ is dominated by other processes.

Figure 2 shows the ${}^6\text{Li}$ yield and major contributions to it, as a function of the antimatter radius, for $R = 0.01$ and $\eta = 6 \times 10^{-10}$. The ${}^6\text{Li}$ production is dominated by nonthermal reaction on ${}^4\text{He}$ by ${}^3\text{H}$ and ${}^3\text{He}$ produced in ${}^4\text{He} + \bar{p}(\bar{n})$ annihilation. The production via ${}^4\text{He}$ photodisintegration becomes important at scales larger than 10^9 m. At scales $r_A < 10^8$ m (annihilation at $T > 10$ keV) ${}^6\text{Li}$ is destroyed via the thermal neutron reaction ${}^6\text{Li} + \text{n} \rightarrow {}^4\text{He} + {}^3\text{H}$.

The rise in the ${}^6\text{Li}$ production at scales 10^7 – 10^8 m is due to the inefficient slowing down of ions at high temperatures, when the thermal velocities of the plasma electrons exceed the velocity of the ion (see [3]). The probability of a nuclear reaction is then higher. Direct production of ${}^6\text{Li}$ through photodisintegration and annihilation of ${}^7\text{Li}$ are negligible effects, both contribute $\sim 0.1\%$ of the total ${}^6\text{Li}$.

For comparison, the yields of ${}^3\text{He}$ (including ${}^3\text{H}$) and D are shown in Fig. 3. Production of D is dominated by ${}^4\text{He} + \bar{p}(\bar{n})$ annihilation. For ${}^3\text{He}$ production, both annihilation and photodisintegration of ${}^4\text{He}$ are important. Spallation of ${}^4\text{He}$ by energetic neutrons contributes less than 10% of the D yield and less than 5% of the ${}^3\text{He}$ yield, and has been omitted from the figure. Photodisintegration is responsible for 0.5% of the destruction of ${}^3\text{He}$ and for 2% of the destruction of D.

C. Diffusion

The mixing of matter and antimatter proceeds through diffusion and collective hydrodynamic flow of the plasma. As different diffusion constants appear in the literature, we present here the constants used in our code.

We use the momentum transfer method [15] to calculate the diffusion constants. Consider the diffusion of a particle species k . The partial pressure of component k is balanced by the force associated with the momentum transfer with other plasma components,

$$-\nabla P_k + \sum_{j \neq k} \mathbf{F}_{kj} = 0. \quad (1)$$

Scattering process	Diffusion constant	cross section	Eq.	statistics
neutron-electron	$D_{ne} = (3/8)(\sqrt{(\pi T/2m_e)/(\sigma_{ne} n_e)})(K_2(z)/K_{2.5}(z))$	$\sigma_{ne} = 8 \times 10^{-4}$ mbarn	6,7	MB
neutron-proton	$D_{np} = (3/8)\sqrt{(\pi T/m_p)/(\sigma_{np} n_p)}$	σ_{np} as in [14]	4	non-rel.
ion-electron	$D_{ie} = (3/4)(m_e^2/(\pi\alpha^2 Z_i^2 \Lambda n_e))(K_2(z)e^z/(z^2 + 2z + 2))$	$\sigma_C(p) = 4\pi\alpha^2\Lambda E^2/p^4$	6,7	MB
ion-ion	$D_{ij} = (3/8)\sqrt{(\pi T)/(2\mu_{ij})}/(\sigma_{pp} Z_i^2 Z_j^2 n_j)$	$\sigma_{pp} = (4\pi\alpha^2\Lambda)/(9T^2)$	4	non-rel.
electron-photon	$D_{e\gamma} = (3/4)T/(\sigma_T \epsilon_\gamma)$	$\sigma_T = 667$ mbarn	6,7	FD

TABLE II. Diffusion constants. $K_n(z)$ is the n th modified Bessel function with $z = m_e/T$.

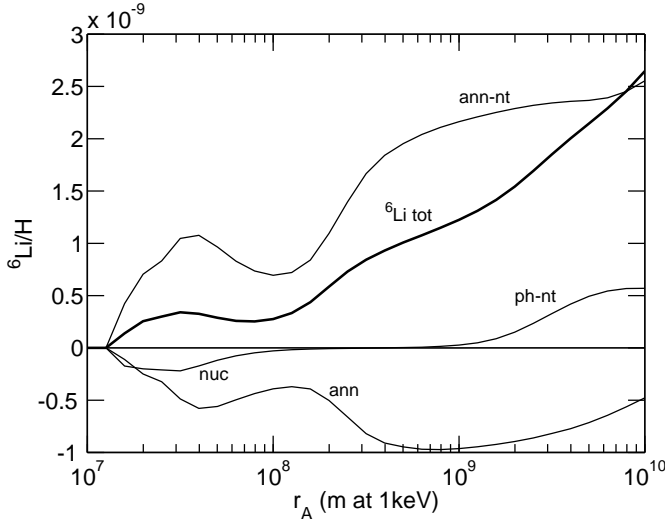


FIG. 2. The ${}^6\text{Li}$ yield and major contributions to it, for $R = 0.01$ and $\eta = 6 \times 10^{-10}$. Shown are the total ${}^6\text{Li}$ yield ('tot'), production via reaction ${}^4\text{He} + {}^3\text{H}({}^3\text{He}) \rightarrow {}^6\text{Li} + \text{n(p)}$ by ${}^3\text{H}$ and ${}^3\text{He}$ ions from annihilation ('ann-nt') and photodisintegration ('ph-nt') of ${}^4\text{He}$. The negative lines show the destruction of ${}^6\text{Li}$ by annihilation ('ann') and thermal ${}^6\text{Li} + \text{n}$ ('nuc').

If both k and j are non-relativistic, the collisional force is given by

$$\mathbf{F}_{kj} = n_k n_j \int \int d^3 \mathbf{u}_k d^3 \mathbf{u}_j f_k(\mathbf{u}_k) f_j(\mathbf{u}_j) |\mathbf{u}_{jk}| \sigma_{kj}^t \mu \mathbf{u}_{jk}, \quad (2)$$

where $f_k(\mathbf{u})$, $f_j(\mathbf{u})$ are the velocity distributions of the two particle species, $\mathbf{u}_{jk} = \mathbf{u}_j - \mathbf{u}_k$ is the relative velocity, μ the reduced mass, and σ_{kj}^t the transport cross section in the center-of-mass frame. Assuming a small deviation from the Maxwellian distribution for k , such that $\langle \mathbf{u}_k \rangle = \mathbf{v}_k$, we obtain

$$\mathbf{F}_{kj} = -n_k n_j \frac{8}{3} \left(\frac{2T\mu}{\pi} \right)^{1/2} \sigma_{kj}^t \mathbf{v}_k. \quad (3)$$

Putting together Eqs. (1) and (2), and the continuity equation, we end up with the diffusion equation, with a diffusion constant equal to

$$D_{kj} = \frac{3}{8} \left(\frac{\pi T}{2\mu} \right)^{1/2} (n_j \sigma_{kj}^t)^{-1} \quad (\text{non-rel.}). \quad (4)$$

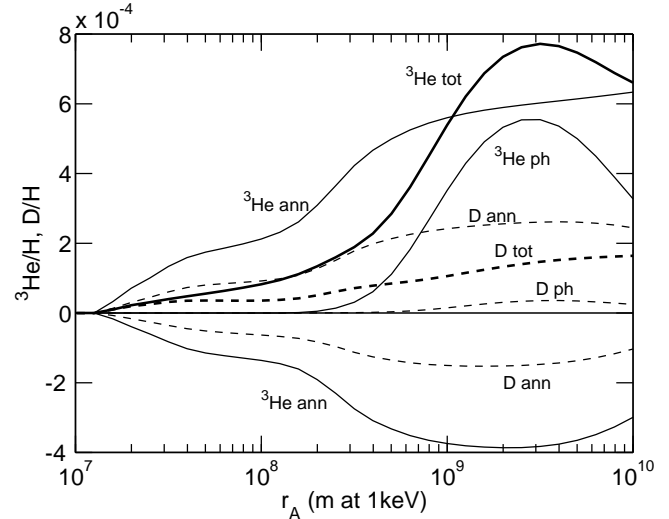


FIG. 3. Major contributions to the production of ${}^3\text{He}$ (solid lines) and D (dashed lines), for $R = 0.01$ and $\eta = 6 \times 10^{-10}$. Shown are the total yield ('tot') from which the SBBN yield has been subtracted, production through annihilation ('ann') and photodisintegration ('ph') of ${}^4\text{He}$, and destruction by annihilation ('ann').

In the case of a heavy non-relativistic gas diffusing into a light relativistic gas the collisional force takes the form

$$\mathbf{F}_{kj} = -\frac{1}{b} n_k \mathbf{v}_k, \quad (5)$$

leading to a diffusion constant

$$D_{kj} = bT \quad (\text{rel.}), \quad (6)$$

where the mobility b is given by

$$-\frac{1}{b} \mathbf{v}_k = \int d^3 \mathbf{p} \rho_j(\mathbf{p}) \frac{|\mathbf{p}|}{E} \sigma_{kj}^t \mathbf{p}. \quad (7)$$

Here ρ_j is the phase space density of particle j in a frame moving with velocity \mathbf{v}_k with respect to the laboratory frame.

We give our diffusion coefficients in table II. In calculating the proton-electron diffusion coefficient, we have integrated over the energy dependence of the Coulomb cross section $\sigma_C(p) = 4\pi\alpha^2\Lambda E^2/p^4$.

Reaction	Threshold	Ref.
${}^6\text{Li} + \gamma \rightarrow {}^4\text{He} + \text{p} + \text{n}$	3.70 MeV	[11]
${}^6\text{Li} + \gamma \rightarrow {}^4\text{He} + \text{D}$	1.48 MeV	[12], not included
${}^7\text{Li} + \gamma \rightarrow {}^6\text{Li} + \text{n}$	7.25 MeV	[11]
${}^7\text{Be} + \gamma \rightarrow {}^6\text{Li} + \text{p}$	5.61 MeV	
${}^7\text{Li} + \gamma \rightarrow {}^4\text{He} + {}^3\text{H}$	2.47 MeV	[13]
${}^7\text{Be} + \gamma \rightarrow {}^4\text{He} + {}^3\text{He}$	1.59 MeV	
${}^7\text{Li} + \gamma \rightarrow {}^4\text{He} + 2\text{n} + \text{p}$	10.96 MeV	[11]
${}^7\text{Be} + \gamma \rightarrow {}^4\text{He} + 2\text{p} + \text{n}$	9.31 MeV	

TABLE I. Photodisintegration channels for nuclei with $A = 6, 7$, with threshold energies and references to the cross-section data. For ${}^7\text{Be}$ we use the ${}^7\text{Li}$ data, shifted in energy according to the threshold energy. Photodisintegration of nuclei with $A \leq 4$ is as in [3].

D. Transfer of energy and momentum

The annihilation of a nucleon-antinucleon pair produces a number of pions (on average 5) which decay into photons, muons and neutrinos. The muons decay further into electrons and neutrinos. Electrons and photons initiate electromagnetic cascades. If one of the annihilating pair is a nucleus, the annihilation leaves nuclear remnants with energies of the order of 10 MeV.

We discussed the spreading of the annihilation products and the electromagnetic cascades in [3]. We ignored the effects on the kinetic behaviour of the plasma, as we estimated them to be small. Here we discuss these effects in more detail.

The annihilation products spreading out from the annihilation zone cause an effective force that tends to push (anti)matter away from the annihilation zone. The kinetic temperature of the plasma, however, is not affected by the energy deposit from the annihilation products, as we will argue below.

The universe is radiation dominated during the era we are interested in. The energy released in annihilation corresponds to a small fraction of the energy in the photon background. The photons form an essentially homogeneous heat bath, which will efficiently dilute the annihilation energy, if only the energy transfer between photons and plasma particles is rapid enough. To see if that is the case, we must compare the energy transfer rate with the annihilation time scale.

In Fig. 4 we plot the annihilation temperature versus the radius of the antimatter region. During the annihilation phase the temperature of the universe typically falls by one decade.

Electrons transfer energy to photons through inverse Compton scattering, or, equivalently, through Thomson drag. The relaxation time for the electron temperature in the photon bath is given by

$$t_{\text{eq}} = \frac{3}{8} \frac{m_e}{\sigma_T \epsilon_\gamma} \approx 1.1 \times 10^{-7} \text{s} \left(\frac{T}{\text{keV}} \right)^{-4}. \quad (8)$$

This is small compared with the annihilation time scale,

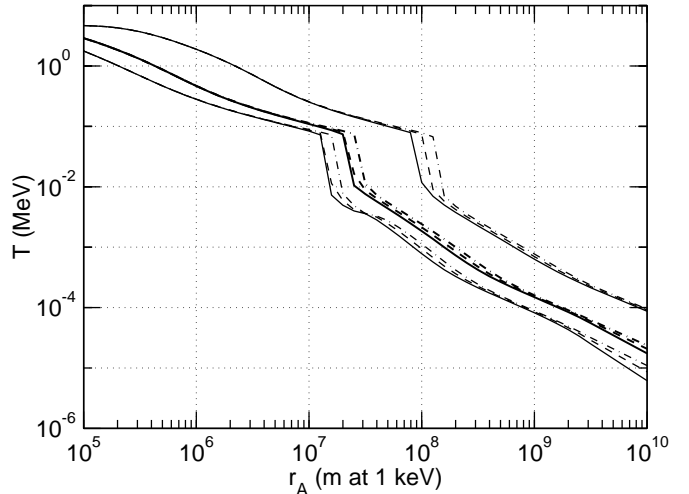


FIG. 4. Annihilation temperature. Shown is the temperature at which 10% (up), 50% (mid), and 90% (down) of antimatter has been annihilated, for $R = 0.01$ and $\eta_{10} \equiv 10^{10} \eta = 9$ (solid), $\eta_{10} = 6$ (dashed) and $\eta_{10} = 4$ (dash-dotted). Before nucleosynthesis the mixing of matter and antimatter proceeds through diffusion of free neutrons. If annihilation is not complete before the onset of nucleosynthesis ($T \approx 80$ keV), it is delayed until proton diffusion becomes effective.

implying that electrons and photons maintain the same temperature.

In the annihilation on a nucleus, a small fraction of the energy is carried away by fragments of the nucleus. The ions are slowed down by Coulomb collisions, first with electrons, and at lower energies with ions. Scattering on ions dominates the slowing down of an ion below energy $E \sim 16T$.

Energy transfer between electrons and ions is inefficient due to their mass difference. When energy is injected into the plasma, a thermal energy distribution is first established within electrons and ions separately, possibly at different kinetic temperatures [16]. The thermalization between ions and electrons then occurs with a relaxation time

$$t_{\text{eq}} = \frac{3}{8\sqrt{2\pi}} \frac{A_i m_p m_e}{n_e Z_i^2 \alpha^2 \Lambda} \left(\frac{T_e}{m_e} \right)^{\frac{3}{2}} \approx 0.2s \frac{A_i}{\eta_{10}} \left(\frac{T_e}{\text{keV}} \right)^{-\frac{3}{2}}. \quad (9)$$

This also is small compared with the annihilation time scale, which implies that ions keep the same temperature with electrons and photons. We may conclude that the effect of the annihilation on the plasma temperature can be neglected.

The annihilation energy may still distort the photon spectrum, leaving an observable remnant in the CMB. The absence of observed distortion constrains the annihilation occurring below 1 keV.

Although the nuclear fragments carry only a small fraction of the annihilation energy, they carry a large fraction of the momentum. The momentum is transferred into the plasma near the annihilation zone via collisions with plasma particles. This causes a force that resists the flow of matter into the annihilation zone. The effective pressure gradient along the radial direction is

$$\nabla P = \int \int f(E, \theta) F(E) \cos \theta d\Omega dE. \quad (10)$$

Here $f(E, \theta)$ is the spectral density of ions flowing into direction θ , $F(E) = dE/dx$ is the energy loss per unit distance due to collisions, and θ is the angle between the ion's velocity and the radial direction.

This effect was implemented into our computer code, but the effect turned out to be negligible. At largest the effect was to reduce by 1% the temperature at which the annihilation is complete.

III. RESULTS

A. Production of isotopes in ABBN

Figure 5 shows the isotope yields for $\eta_{10} \equiv 10^{10} \eta = 4, 6, 9$ and for antimatter fractions $R = 0.01$ and $R = 0.001$.

The ^4He yield is generally reduced in antimatter nucleosynthesis as compared to SBBN. At small scales the reduction is due to annihilation of neutrons before nucleosynthesis, at large scales due to annihilation and photodestruction of ^4He . The relative reduction in ^4He is rather independent of η . Maximal reduction in ^4He is found at scale $r_A \approx 10^7$ m.

Annihilation and photodisintegration of ^4He produce ^3He and D. The final ^3He and D yields are a sum of the SBBN yield and production due to annihilation. The latter depends only weakly on η .

The ^7Li abundance is only weakly affected by annihilation. The small increase in the ^7Li yield at large scales is due to the ordinary inhomogeneity effect: nucleosynthesis takes place at a local density n_b higher than the net baryon density \bar{n}_b .

The ^6Li yield increases in ABBN, as discussed in section II. Like in the case of D and ^3He , the final ^6Li yield is a sum of the SBBN yield and additional production due to annihilation, the latter being only weakly dependent of η .

The yields of D, ^3He , ^6Li , and ^7Li are reduced together with that of ^4He at scales around 10^7 m. The decrease in isotopes other than ^4He is insignificant, except for large antimatter fractions, for which ^4He is severely underproduced. It is not possible in ABBN to significantly reduce D, ^3He , ^6Li , or ^7Li , and simultaneously produce an acceptable ^4He value.

B. Observational constraints

There are two competing estimates for the primordial helium abundance, both based on measurements on the ^4He abundance in extragalactic low-metallicity HII regions. One group obtains $Y_p = 0.234 \pm 0.003$ [17] ("low ^4He "), the other group $Y_p = 0.244 \pm 0.002$ [18] ("high ^4He "). These values correspond, respectively, to $1.2 < \eta_{10} < 2.7$ and $2.7 < \eta_{10} < 5.8$ (2σ limits) in SBBN. Peimbert *et al.* have recently measured $Y = 0.2405 \pm 0.0018$ in the Small Magellanic Cloud, and based on this, estimate $Y_p = 0.2345 \pm 0.0026$ [19].

Burles and Tytler [20] claim to have established the primordial deuterium abundance as $D/H = (3.3 \pm 0.25) \times 10^{-5}$, based on a detected low deuterium abundance in three Lyman absorption systems. Their D/H value gives $5.2 < \eta_{10} < 5.8$ in SBBN. O'Meara *et al.* [21] have recently added a fourth deuterium detection, and revised the combined estimate to $D/H = (3.0 \pm 0.4) \times 10^{-5}$ ($5.4 < \eta_{10} < 6.4$).

A recent review by Steigman [22] suggests observational constraints $0.228 < Y_p < 0.248$ and $2.9 \times 10^{-5} < D/H < 4.0 \times 10^{-5}$. We adopt the ^4He constraints and the upper D limit of Steigman, but we extend the lower D limit to $D/H > 2.2 \times 10^{-5}$ to take into account the O'Meara *et al.* result. These constraints lead to the SBBN estimates $1.2 < \eta_{10} < 5.8$ from Y_p and $4.8 < \eta_{10} < 7.1$ from D/H. We discuss also the implications of the low ^4He estimate.

The best estimate of the primordial lithium abundance is obtained from the "Spite plateau" [23]. Bonifacio and Molaro [24] obtain a present abundance $\log_{10}(^7\text{Li}/\text{H}) = -9.80 \pm 0.012 \pm 0.05$ for the Spite plateau. While a number of authors [25] argue against significant depletion from the primordial abundance, Pinsonneault *et al.* [26] estimate a depletion factor of 0.2–0.4 dex. To be conservative, we adopt the relaxed constraint $^7\text{Li}/\text{H} < 4 \times 10^{-10}$ (SBBN $1.1 < \eta_{10} < 5.9$).

A number of measurements on the $^6\text{Li}/^7\text{Li}$ ratio in halo and disk stars [27] give results ranging from zero up to $^6\text{Li}/^7\text{Li} < 0.13$. Based on this, Jedamzik adopts the tentative limit $^6\text{Li}/\text{H} < 7 \times 10^{-12}$ [5] for the primordial ^6Li . As ^6Li is very fragile and may have been affected by stellar processing, it cannot be ruled out that the primordial ^6Li is significantly higher. We choose to use only the ^4He , D, and ^7Li constraints in determining the allowed range in η .

C. Fitting η

As we have seen, in ABBN the ^4He yield is reduced, and the D yield increased with respect to SBBN. This indicates that we may find consistency with observations at a high baryon density which is not allowed in SBBN.

Figures 6–8 show the observational constraints on the (r_A, R) plane, for different values of η . Shown are the

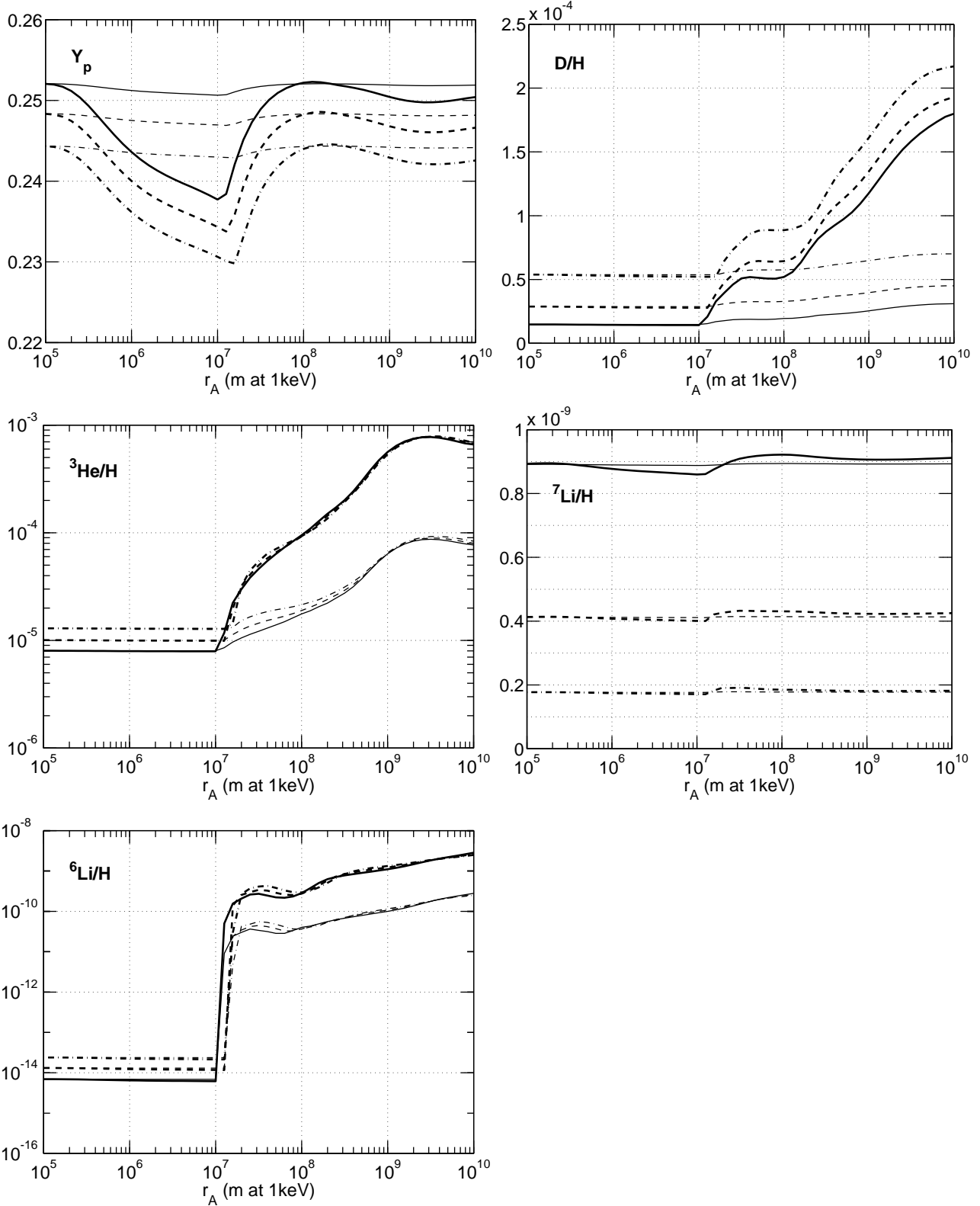


FIG. 5. Isotope yields, versus the radius of the antimatter region, for $\eta = 4 \times 10^{-10}$ (dot-dashed lines), $\eta = 6 \times 10^{-10}$ (dashed lines), and $\eta = 9 \times 10^{-10}$ (solid lines). The thick lines are for antimatter fraction $R = 0.01$, the thin lines for $R = 0.001$. On the left the results converge towards the SBBN yield.

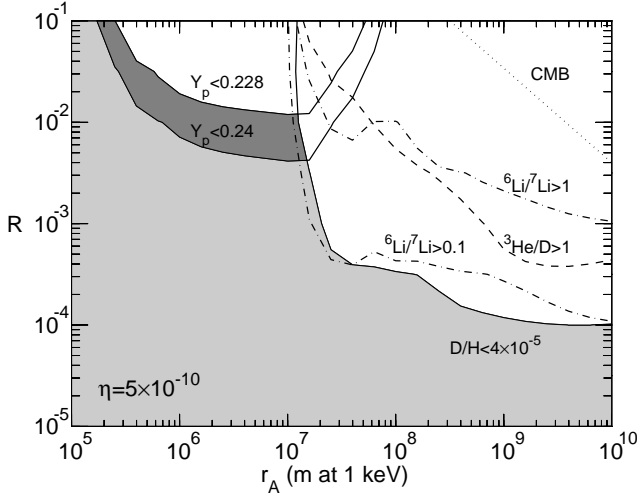


FIG. 6. Observational BBN constraints on the (r_A, R) plane, together with the CMB constraint, for $\eta = 5 \times 10^{-10}$. The lower left corner of the plot corresponds to SBBN. The shadowing indicates regions that satisfy the D and ${}^4\text{He}$ constraints $2.2 \times 10^{-5} < \text{D/H} < 4.0 \times 10^{-5}$, $Y_p > 0.228$, and $Y_p < 0.240$ (dark shading) or $Y_p < 0.248$ (light shading). The ${}^7\text{Li}$ yield (${}^7\text{Li}/\text{H} = 2.8 \times 10^{-10}$) is nearly constant over the parameter plane. For comparison we show also the constraint ${}^3\text{He}/\text{D} < 1$ (dashed line) and the contours ${}^6\text{Li}/{}^7\text{Li} = 0.1$, ${}^6\text{Li}/{}^7\text{Li} = 1$ (dash-dotted lines). The SBBN yields are $\text{D/H} = 3.8 \times 10^{-5}$, ${}^3\text{He}/\text{H} = 1.1 \times 10^{-5}$, $Y_p = 0.2466$, ${}^6\text{Li}/\text{H} = 1.7 \times 10^{-14}$, and ${}^7\text{Li}/\text{H} = 2.8 \times 10^{-10}$.

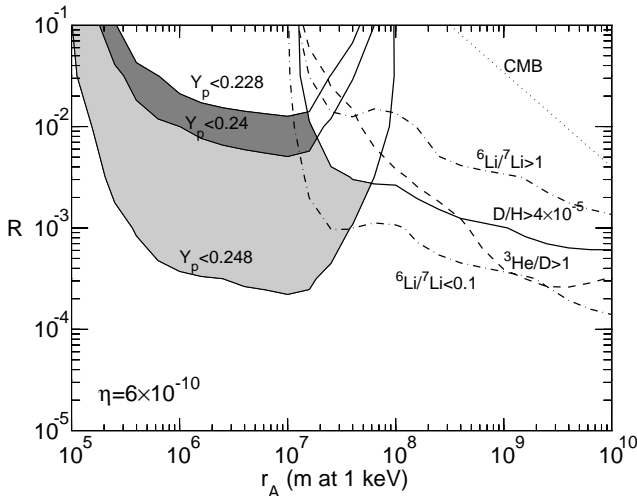


FIG. 7. Same as Fig. 6, but for $\eta = 6 \times 10^{-10}$. The ${}^7\text{Li}$ yield is ${}^7\text{Li}/\text{H} = 4.1 \times 10^{-10}$. The SBBN yields are $\text{D/H} = 2.9 \times 10^{-5}$, ${}^3\text{He}/\text{H} = 1.0 \times 10^{-5}$, $Y_p = 0.2483$, ${}^6\text{Li}/\text{H} = 1.3 \times 10^{-14}$, and ${}^7\text{Li}/\text{H} = 4.1 \times 10^{-10}$.

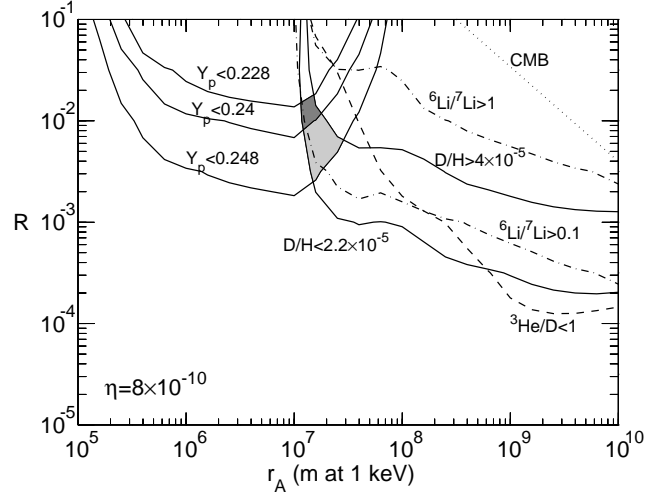


FIG. 8. Same as Fig. 6, but for $\eta = 8 \times 10^{-10}$. The D and ${}^4\text{He}$ constraints are satisfied in the shadowed region. However, this high a baryon density is excluded by overproduction of ${}^7\text{Li}$, whose yield ${}^7\text{Li}/\text{H} = 7.3 \times 10^{-10}$ is constant over the plane. The SBBN yields are $\text{D/H} = 1.8 \times 10^{-5}$, ${}^3\text{He}/\text{H} = 8.6 \times 10^{-6}$, $Y_p = 0.2510$, ${}^6\text{Li}/\text{H} = 8.4 \times 10^{-15}$, and ${}^7\text{Li}/\text{H} = 7.3 \times 10^{-10}$.

constraints $2.2 \times 10^{-5} < \text{D/H} < 4.0 \times 10^{-5}$ and $0.228 < Y_p < 0.248$, $Y_p < 0.240$. For comparison we show also the constraint ${}^3\text{He}/\text{D} < 1$ used in [3] and the contours ${}^6\text{Li}/{}^7\text{Li} = 0.1$ and ${}^6\text{Li}/{}^7\text{Li} = 1$. The yield of ${}^7\text{Li}$ is nearly constant over the plane, and is therefore not shown as contours. The CMB constraint is obtained by demanding that the energy released in annihilation must not exceed a fraction of 6×10^{-5} of the CMB energy.

Figure 6 shows our results for $\eta = 5 \times 10^{-10}$ ($\Omega_b h^2 = 0.0182$). The value $\eta_{10} = 5$ is consistent with observations in SBBN, if we accept the high ${}^4\text{He}$ limit, $Y_p < 0.248$. The low ${}^4\text{He}$ limit, $Y_p < 0.240$ is inconsistent with the deuterium yield in SBBN, but in ABBN we find a consistency region at $R > 0.004$, at scales $r_A < 10^7$ m. The constraints $Y_p < 0.248$ and $\text{D/H} > 2.2 \times 10^{-5}$ are satisfied everywhere in the parameter plane.

In Fig. 7 we show our results for $\eta = 6 \times 10^{-10}$ ($\Omega_b h^2 = 0.0219$). This value is excluded in SBBN by overproduction of ${}^4\text{He}$ (SBBN yield $Y_p = 0.2483$). Lithium-7 (${}^7\text{Li}/\text{H} = 4.1 \times 10^{-10}$) is slightly above its upper limit. In ABBN there is a region in the parameter space, where both ${}^4\text{He}$ and D are well in their observed ranges. The required antimatter fraction depends on which Y_p limit we adopt. We find $R > 2 \times 10^{-4}$ for $Y_p < 0.248$ and $R > 0.005$ for $Y_p < 0.240$. The ${}^7\text{Li}$ yield, however, remains close to its SBBN value, and is only marginally acceptable.

Figure 8 shows our results for $\eta = 8 \times 10^{-10}$ ($\Omega_b h^2 = 0.0292$). The ${}^7\text{Li}$ yield ${}^7\text{Li}/\text{H} = 7.3 \times 10^{-10}$ is clearly inconsistent with the present estimations of the primordial ${}^7\text{Li}$ abundance. Still, it is interesting to

note that it is possible to bring both D and ^4He into their observed ranges. In the region allowed by the D and ^4He constraints the $^6\text{Li}/^7\text{Li}$ ratio varies in the range $0.06 - 0.4$.

Overproduction of deuterium sets a lower limit to the baryon density which can be accommodated in ABBN. Since ABBN cannot reduce the D/H yield from the SBBN yield, without simultaneously severely underproducing ^4He , a low baryon density that is excluded in SBBN by D/H overproduction is excluded in ABBN as well. With our adopted observational constraints ($\text{D/H} < 4.0 \times 10^{-5}$) this gives a lower limit $\eta > 4.8 \times 10^{-10}$, corresponding to $\Omega_b h^2 > 0.0177$.

An upper limit to η is obtained from overproduction of ^7Li , whose yield in ABBN is not significantly deviated from SBBN. With $^7\text{Li}/\text{H} < 4 \times 10^{-10}$ we get $\eta < 5.9 \times 10^{-10}$ ($\Omega_b h^2 < 0.0216$). Thus the range allowed for η by our adopted observational constraints changes only slightly, from $4.8 < \eta_{10} < 5.8$ in SBBN to $4.8 < \eta_{10} < 5.9$ in ABBN.

Recent balloon experiments on CMB anisotropy, Boomerang and Maxima-1, suggest a large baryon density $\Omega_b h^2 \sim 0.030$, $\eta \sim 8 \times 10^{-10}$ [28] in clear conflict with SBBN. Antimatter nucleosynthesis alone is not a solution for this discrepancy, because of the overproduction of lithium at large η . It can, however, help with D and ^4He .

In [2,3] we placed upper limits on the antimatter fraction at $\eta = 6 \times 10^{-10}$. Our new results show that the limit is not sensitive to the value of η .

IV. CONCLUSIONS

Nucleosynthesis in the presence of antimatter can produce simultaneously a small ^4He mass fraction and a high D/H ratio, allowing for a higher baryon density than SBBN. Antimatter nucleosynthesis provides one possible solution to the discrepancy between the low primordial ^4He value suggested by some observations and the low D/H value.

The allowed baryon density is limited from above by ^7Li overproduction. The ^7Li yield is almost unaffected by the presence of antimatter. A baryon density larger than $\Omega_b h^2 = 0.0216$ leads to a high lithium yield $^7\text{Li}/\text{H} > 4 \times 10^{-10}$, in conflict with the present estimates of the primordial value.

Since the ^7Li yield is almost unaffected by ABBN, the upper limit to Ω_b is not much changed from SBBN. However, if one disregards the ^7Li limit, ABBN allows larger values of Ω_b than SBBN, including the high value suggested by Boomerang and Maxima-1.

ACKNOWLEDGEMENTS

I thank H. Kurki-Suonio for useful discussions, and the Center for Scientific Computing (Finland) for computational resources.

* Electronic address: Elina.Sihvola@helsinki.fi

- [1] J.B. Rehm and K. Jedamzik, Phys. Rev. Lett. **81**, 3307 (1998).
- [2] H. Kurki-Suonio and E. Sihvola, Phys. Rev. Lett. **84**, 3756 (2000).
- [3] H. Kurki-Suonio and E. Sihvola, Phys. Rev. D **62**, 103508 (2000).
- [4] J.B. Rehm and K. Jedamzik, Phys. Rev. D **63**, 043509 (2001).
- [5] K. Jedamzik, Phys. Rev. Lett. **84**, 3248 (2000).
- [6] M. Kawasaki, K. Kohri, and T. Moroi, astro-ph/0012279.
- [7] J.A. Koepke and R.E. Brown, Phys. Rev. C **16**, 18 (1977).
- [8] J.C. Overley, R.M. Sealock, and D.H. Ehlers, Nucl. Phys. **A221**, 573 (1974).
- [9] C.M. Bartle, Nucl. Phys. **A330**, 1 (1974).
- [10] C.M. Bartle, D.W. Gebbie, and C.L. Hollas, Nucl. Phys. **A397**, 21 (1983).
- [11] S.S. Dietrich and B.L. Berman, At. Data and Nucl. Data Tables **38**, 199 (1988).
- [12] R.G.H. Robertson *et al.*, Phys. Rev. Lett. **47**, 1867 (1981).
- [13] D.M. Skopik, J. Asai, E.L. Tomusiak, and J.J. Murphy II, Phys. Rev. C **20**, 2025 (1979).
- [14] J.H. Applegate, C.J. Hogan, and R.J. Scherrer, Phys. Rev. D **35**, 1151 (1987).
- [15] See, e.g., R.D. Present, *Kinetic Theory of Gases*, (McGraw-Hill Book Company, New York, 1958).
- [16] L. Spitzer, Jr., *Physics of Fully Ionized Gases* (Interscience Publishers, New York, 1956).
- [17] K.A. Olive and G. Steigman, Astrophys. J. Supp. S. **97**, 49 (1995); K.A. Olive, G. Steigman, and E.D. Skillman, Astrophys. J. **483**, 788 (1997).
- [18] Y.I. Izotov, T.X. Thuan, and V.A. Lipovetsky, Astrophys. J. **435**, 647 (1994); Astrophys. J. Supp. S. **108**, 1 (1997); Y.I. Izotov and T.X. Thuan, Astrophys. J. **500**, 188 (1998).
- [19] M. Peimbert, A. Peimbert, and M.T. Ruiz, Astrophys. J. **541**, 688 (2000).
- [20] S. Burles and D. Tytler, Astrophys. J. **499**, 699 (1998); **507**, 732 (1998).
- [21] J.M. O'Meara, D. Tytler, D. Kirkman, N. Suzuki, J.X. Prochaska, D. Lubin, and A.M. Wolfe, astro-ph/0011179.
- [22] G. Steigman, astro-ph/0009506.
- [23] M. Spite and F. Spite, Astron. Astrophys. **115**, 357 (1982); Nature **297**, 483 (1982).
- [24] P. Bonifacio and P. Molaro, Mon. Not. R. Astron. Soc. **285**, 847 (1997).
- [25] S.G. Ryan, J.E. Norris, and T.C. Beers, Astrophys. J.

523, 654 (1999); S.G. Ryan, T.C. Beers, K.A. Olive, B.D. Fields, and J.E. Norris, *Astrophys. J. Lett.* **530**, L57 (2000); T.K. Suzuki, Y. Yoshii, and T.C. Beers, *Astrophys. J.* **540**, 99 (2000).

[26] M.H. Pinsonneault, T.P. Walker, G. Steigman, and V.K. Narayanan, *Astrophys. J.* **527**, 180 (1999).

[27] L.M. Hobbs and J.A. Thorburn, *Astrophys. J.* **491**, 772 (1997); R. Cayrel, M. Spite, F. Spite, E. Vangioni-Flam, M. Cass, and J. Audouze, *Astron. Astrophys.* **343**, 923 (1999); V.V. Smith, D.L. Lambert, and P.E. Nissen, *Astrophys. J.* **506**, 405 (1998); P.E. Nissen, D.L. Lambert, F. Primas, and V.V. Smith, *Astron. Astrophys.* **348**, 211 (1999).

[28] A. Balbi *et al.*, *Astrophys. J.* **545**, L1 (2000); A.E. Lange *et al.*, astro-ph/0005004; A.H. Jaffe *et al.*, astro-ph/0007333; J.R. Bond *et al.*, astro-ph/0011378.